Design and Characterisation of a FRET-Based Biosensor for Intracellular Calcium Detection

BGN: 2265V

30th January 2025

Practical Course - Lab Report

Word Count - 1946

Course Demonstrators: Wenyue Dai, Hassan Rahmoune, Ana Pascual Garrigos, Aishwarya Venkatramani, Maria Lopez Cavestany, Edward Ward

Contents

Abstract

The objective of this report is to construct and characterise a calcium biosensor using a Förster resonance energy transfer (FRET)-based approach. The D3cpv sensor was assembled via Gibson Assembly, expressed in E. coli, and purified using nickel affinity chromatography. Fluorescence-based assays and fluorescence lifetime imaging microscopy (FLIM) was employed to validate the functional response of the biosensor in HeLa cells. While sequencing confirmed successful cloning, issues such as bacterial transformation failures and assay contamination affected the final analysis. This study highlights the challenges and potential of FRET-based biosensors.

1 Introduction

Calcium ions (Ca^{2+}) play a crucial role in intracellular signalling, regulating gene expression, muscle contraction, neurotransmitter release, and apoptosis. As a second messenger, transient changes in intracellular calcium concentration activate calcium-binding proteins such as calmodulin, influencing key biological processes. Disruptions in calcium homeostasis are linked to neurodegeneration, cancer, and cardiovascular disease [1]. Genetically encoded calcium indicators (GECIs), such as FRET-based biosensors, offer a non-invasive and dynamic approach to measuring intracellular calcium.

This study aimed to develop a FRET-based D3cpv calcium biosensor. Molecular cloning techniques were used to assemble the construct, which was expressed in E. coli and purified using nickel affinity chromatography. Fluorescence-based calcium titration and FLIM were employed to assess its functionality in HeLa cells. By assessing biosensor design and experimental protocols, this study explores the potential of GECIs for real-time intracellular calcium measurement.

2 Biotechnological Interest of Intracellular Calcium Sensing

Calcium ions (Ca^{2+}) play a fundamental role as intracellular messengers, orchestrating various biological processes such as signal transduction, gene expression, and enzymatic regulation [2]. The versatility of Ca^{2+} signalling stems from its ability to generate highly specific spatio-temporal patterns that regulate physiological responses, including neurotransmission, muscle contraction, and immune activation [3]. In biotechnology, GECIs have revolutionised the study of Ca^{2+} dynamics, providing real-time insights into cellular function [4]. These biosensors, based on FRET or single-wavelength fluorophores, enable non-invasive monitoring of Ca^{2+} fluctuations in live cells, advancing research in neurobiology and pharmacology. Additionally, in plant biotechnology, calcium homeostasis is essential for stress adaptation and environmental resilience, influencing drought resistance and heavy metal detoxification [5]. The engineering of calcium-sensitive pathways offers promising applications in synthetic biology, bioengineering, and therapeutic interventions.

3 Methodology

3.1 Molecular Cloning

The Gibson Assembly approach used three fragments: CFP and YFP from pcDNA-D3CPV, and the linearised pET24a backbone from pET24. Each had forward and reverse primers, with expected amplicon sizes of 803, 1225, and 5234 bp respectively. PCR was performed using 20 ng of template DNA, Q5 High-Fidelity polymerase, and fragment-specific primers under standard denaturing, annealing, and extension cycles (extension time 1 min 45 s, see Appendix 5). Agarose gel electrophoresis was employed for product quantification (Section 4). DpnI digestion removed methylated parental DNA (from E. coli) to select newly synthesised DNA.

3.2 Assembly and Verification

Purified DNA fragments were assembled by Gibson Assembly in a 2:2:1 ratio of CFP:YFP:pET24, with 50 ng of pET24a vector. The mixture was incubated at 50 °C for ˜60 minutes and cooled for 5 minutes, then 5 µL was transformed into 50 µL of E. coli by heat shock at 42 °C for 30 seconds. After recovery in SOB, cells were plated on LB agar containing 50 µg mL^{-1} kanamycin. Colony PCR used promoter and terminator primers, yielding a 2142 bp product for correct inserts and 259 bp for empty vectors. Attempts to grow colonies were compromised by contamination, so results from alternative plates were used. Verified colonies were grown overnight in LB-kanamycin at 37 °C with shaking.

3.3 Protein Purification, Production and Characterisation

Overnight E. coli cultures were treated with RNase A and lysed, and plasmid DNA was purified using a QIAGEN kit. NanoDrop measurements and outsourced sequencing (Section 4) assessed DNA quality. For protein expression, 5 mL of overnight culture was used to inoculate 400 mL of LB with 50 µg mL^{-1} kanamycin. Cells were grown at 37 °C (200 RPM), and optical density (600 nm) was monitored hourly to identify the active log phase. IPTG was introduced, and cultures were incubated further at 37 °C, followed by SDS-PAGE analysis (Section 4). Pelleted cells were lysed and clarified by centrifugation and 0.45 µm filtration. Nickel affinity chromatography (using an imidazole gradient) purified the His-tagged D3cpv sensor, which was then buffer-exchanged into MOPS. A fluorescence assay aiming to determine the sensor's dissociation constant (K_d) across a 0.01 mM – 2000 mM Ca^{2+} concentration gradient was inconclusive due to suspected EGTA contamination.

3.4 Cell Culture and Microscopy

HeLa cells were maintained in DMEM with FBS and antibiotics. After trypsinisation, approximately 10,000 cells were seeded per well (eight wells total). Transfections via Lipofectamine 2000 included: wild type (pcDNA-D3cpv), mutant (pcDNA-CFP), wild

type + CRISPR CALM2 (1:1 pcDNA-D3cpv : Purocymin-Cas9-gRNA-1), and wild type + drug. Cells were incubated at 37 °C. An ideal incubation period would be ˜3 days, however due to time limitations of the experiment, cells were incubated for 18–24 hours. FLIM was used to measure FRET changes upon Ca^2+ binding, and FLIMFit software distinguished interacting from non-interacting protein states (Section 4).

4 Results and Discussion

4.1 Molecular Cloning

In Silico Design of pET24-D3cpv Construct

he construct was designed in silico using Benchling:

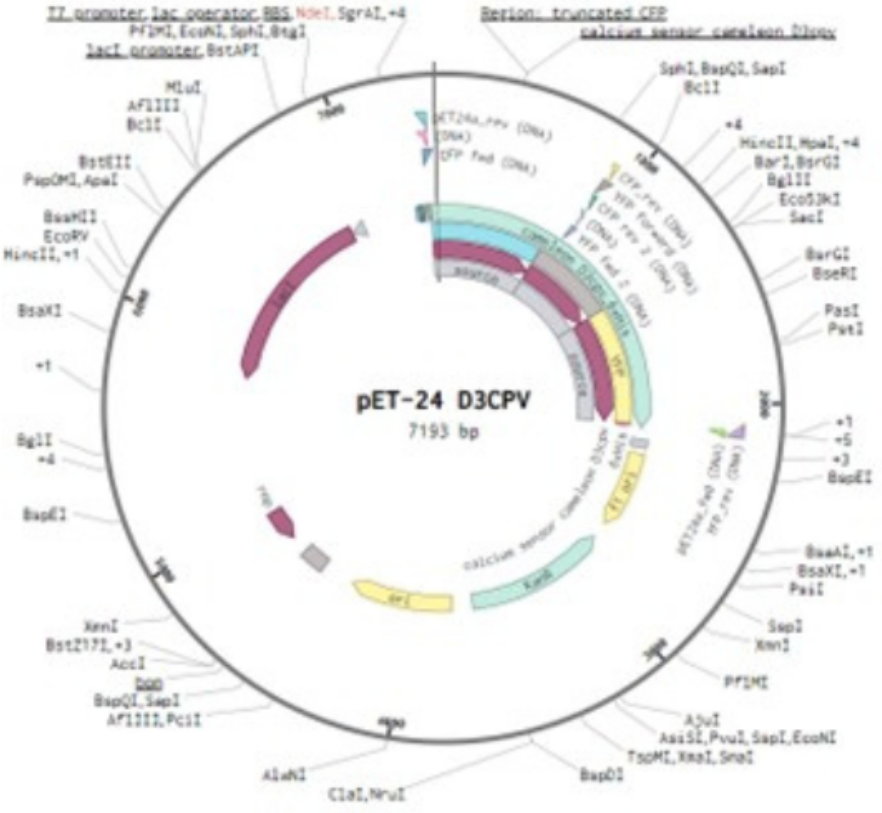

Figure 1: pET24a D3CPV Construct, with length 7193 bp

To form a calcium sensor, the calcium-sensing D3cpv domain from pcDNA-D3cpv was designed into the bacterial expression vector from the pET24a. The final construct, of size 7193bp, included multiple other essential elements for proceeding experiments. The

LacI and T7 elements allowed for inducible expression in the presence of IPTG, which will be detailed later. The inclusion of an antiobiotic resistance gene (specifically kanamycin) allowed for screening of insertion. The ori of replication allowed for cell culturing.

Primers must be designed for both forwards and backwards reactions. Primers should have 40-60% GC so as to not form secondary structures and to bind to the correct part of the plasmid. As can be seen in Table 1, all primers (aside from pET24a rev) had an appropriate GC content and Tm (Melting Temperature). This may have affected the binding ability of the pET24a rev primer during PCR reactions.

Primer	**Tm (°C)**	**Length (bp)**	**GC content (%)**
pET24a forward	67.4	28	64.29
pET24a rev	55.4	41	21.95
CFP forward	66.9	45	44.44
CFP rev	62.2	23	60.87
YFP forward	74.5	44	59.09
YFP rev	63.3	29	51.72

Table 1: Primer properties including melting temperature (Tm), length, and GC content.

PCR Amplification of CFP and YFP Fragments

Using a Gibson Assembly method, PCR amplification of the CFP and YFP sequences was attempted. To quantify the performance of this method, a gel electrophoresis was performed in 4 columns: a DNA ladder, CFP fragment, YFP fragment and the pET24a. Further analysis came from the use of a NanoDrop machine. This is a specialised spectrophotometer, used for quantifying and assessing the purity of nucleic acids and proteins in very small sample volumes.

Gel electrophoresis resulted in no visible bands under UV illumination. This outcome may be attributed to samples running off the gel due to improper loading or excessive electrophoresis time, or the absence of CyberSafe dye during gel preparation, preventing nucleic acid visualisation.

Despite the failure of gel electrophoresis, NanoDrop analysis confirmed the presence of nucleic acids in all samples. As seen in Table 2, CFP (48.2 ng/µL) and YFP (16.8

Sample	Nucleic Acid Conc. (ng/µL)	A260/A280 Ratio
CFP	48.2	1.90
YFP	16.8	1.84
pET24a	24.5	1.79

Table 2: NanoDrop quantification results for CFP, YFP, and pET24a samples.

ng/µL) showed measurable concentrations, suggesting successful PCR amplification. The A260/A280 ratios (1.79–1.90) indicate relatively pure DNA, supporting this conclusion. The absence of bands on the gel was likely due to technical issues, described earlier. This exhibits the value of multiple quantification steps. Further experimentation could have been performed to analyse the relatively smaller A260/A280 ratio of the pET24a backbone. This was most likey due to inadequate PCR clean-up, causing residual salts or protein contamination.

4.2 Assembly and Verification

Colony PCR Analysis

Colony PCR was performed to screen for successful transformants following Gibson Assembly. The control sample showed no amplification, confirming that the primers were specific to the recombinant construct. As visual inspection of the gel electrophoresis can be inconclusive, the bright bands consistently shown across the colonies may fall between 600-700bp. To consider the 700bp case, this would mean a successful transformation of CFP across all colonies. Considering the case with 600bp, either only a partial insert was incorporated, or PCR preferentially amplified a shorter region, possibly due to mispriming or suboptimal amplification conditions. Another possible explanation is incomplete washing of DpnI, leading to residual linearised vector or unintended amplification of a background fragment. The presence of different colony PCR results highlights potential heterogeneity in the transformant population, with some clones carrying partial constructs instead of the fully assembled CFP-YFP fusion. Further verification through restriction digestion and sequencing is required to confirm insert integrity.

Sequencing Verification

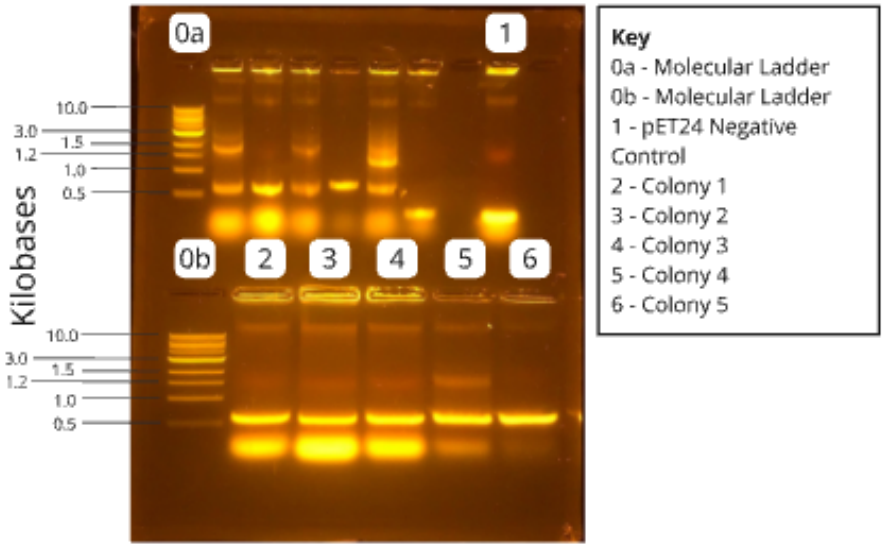

Figure 2: Gel electrophoresis of 5 colony PCR products, two molecular ladders and the pET24a negative control.

An external service was used to validate the sequencing of the construct. The pair-wise identity was high for both the forward and reverse sequences: 96.88% and 97.3% respectively. Hence, the sequencing was validated, confirming that the assembled construct largely matched the expected sequence with only minor discrepancies. These variations could be attributed to sequencing errors, PCR-induced mutations, or minor recombination events during Gibson Assembly. However, the high sequence identity suggests that the construct remained functionally intact, supporting the successful cloning and expression of the target protein.

4.3 Protein Production, Purification and Characterisation

Bacterial Expression and Induction

IPTG induction was performed when the optical density (OD) reached between 0.4 to 0.8. After receiving a value of 0.616OD, IPTG was introduced. A sample was taken before and after IPTG induction. These samples were analysed in an SDS-PAGE, as seen in Figure 3.

The presence of distinct bands at approximately 27 kDa (corresponding to the molecular weight of the target protein) in the post IPTG introduction column confirms successful

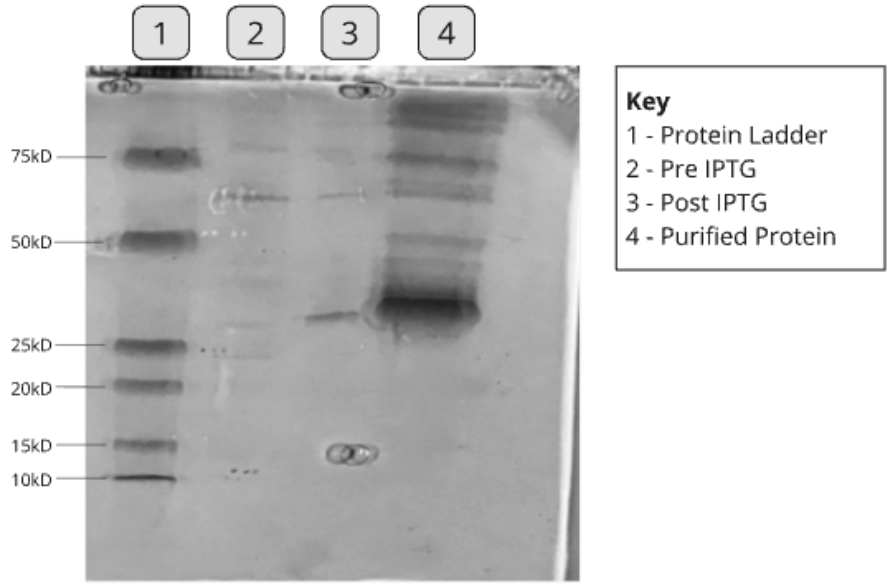

Figure 3: SDS-PAGE of Pre and post IPTG Induction for Protein Expression

bacterial expression of the target protein. This indicates that the construct was correctly expressed in E. coli.

In Vitro Calcium Titration Assay

Due to suspected EGTA contamination, the assays results were unable to be used. The expectation would be for the purified D3cpv sensor to exhibit clear FRET changes, with emission ratios increasing across calcium concentration ranges. A strong fit would be indicated by an R^2 value greater than 0.90. The fitted dissociation constant (K_d) would quantify calcium affinity, with a lower K_d indicating a higher affinity for calcium. The Hill coefficient (n) would describe the cooperativity of calcium binding, where values greater than 1 suggest positive cooperativity, values near 1 indicate independent binding, and values less than 1 suggest negative cooperativity or partial saturation. Controls would be expected to show no response which would confirm calcium dependence.

4.4 Cellular Implementation

FLIM Analysis of Sensor in HeLa Cells

The results for the FLIM analysis can be seen in Table 3. As shown, there is an increase in

E, indicating greater FRET efficiency and, consequently, higher energy transfer between fluorophores. The theoretical range of values for E is between 0% and 100%, hence the result for Wild-Type + CRISPR is an error. This may have been due to fitting errors, background subtraction issues, or donor photophysical effects. Due to the consistency of these issues across different samples, the relative difference between E values of Wild-Type + CRISPR and Mutant may be considered. The higher E observed in the CRISPR condition is attributed to the CALM2 knockout, which likely enhances calcium binding due to reduced calmodulin interference. Since calmodulin normally buffers intracellular calcium levels, its absence could increase local calcium availability, leading to stronger interaction of the calcium sensor and higher FRET efficiency. Further details of FLIM justifications can be found in Appendix H.

Due to time limitations, only 2 of the 4 conditions were analysed using FLIM, with no data for Wild-Type or BAPTA conditions. The expectation for these values would be that the BAPTA treated condition would have the lowest E, due to BAPTA binding and removing calcium. Using the FLIMFit software, a false-colour fluorescence-lifetime map was taken (Figure 4). The top row images show the CRISPR condition, and the bottom row images show the mutant sensor condition. The colour scale encodes fluorescenc lifetimes at each pixel, with cooler colours representing shorter lifetimes and warmer colours indicating longer lifetimes. Higher fluorescence lifetimes can reflect changes in protein conformation or interactions, such as those influenced by altered Ca^{2+} binding.

Condition	**E**	**Mean Lifetime (ns)**
Wild-Type + CRISPR (2024)	107.11%	2.87
Mutant Sensor (2024)	84.25%	2.22

Table 3: FRET Efficiency and Mean Lifetime for Different Conditions

5 Conclusion

The objective of this laboratory session was to engineer and evaluate a FRET-based D3cpv biosensor for measuring intracellular Ca^{2+}. Construction involved Gibson Assembly of CFP, YFP, and pET24a fragments, followed by confirmation through colony

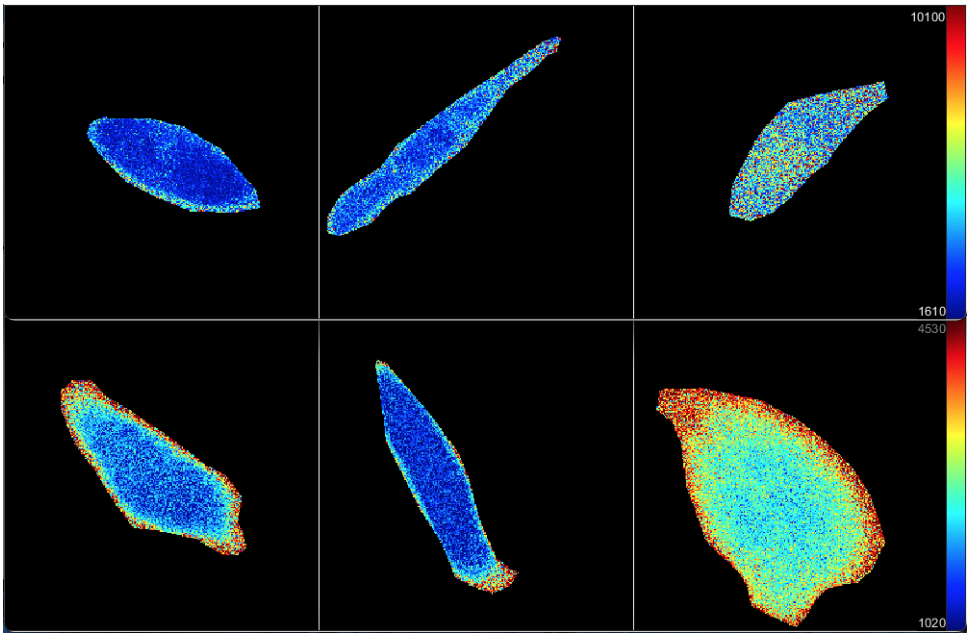

Figure 4: 3 HeLa cells from both the CRISPR (Top) and Mutant (Bottom) Fluorescence Heat Map

PCR, sequencing, and NanoDrop measurements. Although occasional transformation failures and contamination affected colony selection, sequence analysis indicated high fidelity of the final construct. Subsequent expression in E. coli and purification using nickel affinity chromatography demonstrated successful production of the target protein. While the in vitro fluorescence assay could not be completed due to suspected reagent contamination, FLIM analyses in HeLa cells indicated the biosensor's potential to detect variations in Ca^{2+} levels. This was particularly evident in the CRISPR condition, which showed higher FRET efficiency, likely due to reduced calmodulin activity. Future work should optimise transformation efficiency, improve reagent quality control, and expand cellular assays to refine biosensor sensitivity and specificity for broader biotechnological applications.

Appendices

Appendix A

PCR Reaction Components for Initial PCR

Component	Final Concentration	Volume Required for 50 µL Reaction
Q5 High-Fidelity 2X Master Mix	1X	25 µL
10 µM Forward Primer	0.5 µM	2.5 µL
10 µM Reverse Primer	0.5 µM	2.5 µL
20 ng/μL Template DNA		1 µL
Water		19 µL

Table 4: PCR Reactant Components

Appendix B

PCR Cycling Table

Temperature (°C)	Time (s)	Cycles	Phase
98	60	1	Initial denaturing
98	15	25	Denature
60	15		Anneal
72	10		Extension
72	60	1	Final elongation
10	∞	1	Cooling

Table 5: PCR cycling conditions

Appendix C

Extension Time Calculation

Q5 Polymerase requires ˜20s extension time for each 1000bp length. As the longest amplicon is the pET24a backbone, at 5234bp, as the longest amplicon is used to determine the entire extension time, the calculation is $5234/1000 = 5.234$, then $5.234 \times 20s = 104.68s \approx 105s = 1$ minute 45 seconds. Hence, the total extension period for this PCR reaction is 1 1 minute 45 seconds.

Appendix D

Assembly Reaction Components

Appendix E

Colony PCR Preparation

Component	**Concentration** $\mathrm{ng\,\mu L^{-1}}$	**DNA Mass** ng	**Volumes** µL
pET24a	50.0	50.0	1
CFP fragment	14.9	15.3	1
YFP fragment	22.9	23.4	1
2X HiFi Assembly Master Mix			5
Water (up to 10 µL)			2
		Final volume:	**10**

Table 6: Component volumes for assembly reaction

Component	Final Concentration	Volume for 25 µL Reaction (µL)	Number of Reactions	Volume for MasterMix (µL)
5X Reaction buffer	1X	5.0	7	35.0
10 mM dNTPs	200 µM	2.5	7	3.5
5 U/µL OneTaq HotStart	0.025 U/µL	0.125	7	0.9
10 µM forward primer	0.5 µM	1.25	7	8.8
10 µM reverse primer	0.5 µM	1.25	7	8.8
Template				
Water (up to 25 µL)	-	16.875	7	118.1

Table 7: PCR reaction components and master mix preparation

Appendix F

Colony PCR Cycling Table

Temperature (°C)	**Time (s)**	**Cycles**	**Phase**
94	30	1	Initial denaturing
94	15	25	Denature
57	15		Anneal
68	60-120		Extension
68	60	1	Final elongation
10	∞	1	Cooling

Table 8: PCR cycling conditions

Appendix G

IPTG Calculations

To calculate the amount of 1 M IPTG to add to 400 mL of cells to have a final con-

centration of 1 µM, the formula $C_i \times V_i = C_f \times V_f$ can be used. Here C_i = the initial concentration of IPTG, C_f = the desired final concentration , and V_f = the final volume. Hence, $V_i = 571$ µL of IPTG was used.

Appendix H

FRET Efficiency Details

Förster resonance energy transfer (FRET) efficiency (E), quantifies the proportion of energy transferred from a donor fluorophore to an acceptor fluorophore. The FRET efficiency is defined as: $E = 1 - \frac{\tau_D}{\tau_{DA}}$, where τ_D is the fluorescence lifetime of the donor fluorophore in the absence of the acceptor and τ_{DA} is the fluorescence lifetime of the donor in the presence of the acceptor. Higher E values indicate stronger FRET interactions, whereas lower E values suggest greater separation.

References

[1] M. J. Berridge, M. D. Bootman and H. L. Roderick, "Calcium signalling: Dynamics, homeostasis and remodelling," *Nature Reviews Molecular Cell Biology*, vol. 4, no. 7, pp. 517–529, Jul. 2003. DOI: 10.1038/nrm1155.

[2] M. J. Berridge, P. Lipp and M. D. Bootman, "The versatility and universality of calcium signalling," *Nature Reviews Molecular Cell Biology*, vol. 1, pp. 11–21, 2000. DOI: 10.1038/35036035.

[3] A. Miyawaki, "Fluorescent proteins in a new light," *Nature Biotechnology*, vol. 22, pp. 1374–1376, 2004.

[4] A. E. Palmer, M. Giacomello, T. Kortemme *et al.*, "Ca2+ indicators based on computationally redesigned calmodulin-peptide pairs," *Chemistry & Biology*, vol. 13, no. 5, pp. 521–530, 2006.

[5] R. Shabbir, T. Javed, S. Hussain *et al.*, "Calcium homeostasis and potential roles in combatting environmental stresses in plants," *South African Journal of Botany*, vol. 148, pp. 683–693, 2022. DOI: 10.1016/j.sajb.2022.05.038.